Experimental and Theoretical Studies of the Kinetics of the Reactions of OH and OD with 2-Methyl-3-buten-2-ol between 300 and 415 K at Low Pressure

Munkhbayar Baasandorj and Philip S. Stevens*

Institute for Research in Environmental Science, School of Public and Environmental Affairs, and Department of Chemistry, Indiana University, Bloomington, Indiana 47405

Received: September 25, 2006; In Final Form: November 14, 2006

The rate constants for the reactions of OH and OD with 2-methyl-3-buten-2-ol (MBO) have been measured at 2, 3, and 5 Torr total pressure over the temperature range 300−415 K using a discharge-flow system coupled with laser induced fluorescence detection of OH. The measured rate constants at room temperature and 5 Torr for the OH + MBO reaction in the presence of O_2 and the OD + MBO reaction are (6.32 ± 0.27) and (6.61 ± 0.66) × 10^{-11} cm^3 $molecule^{-1}$ s^{-1}, respectively, in agreement with previous measurements at higher pressures. However, the rate constants begin to show a pressure dependence at temperatures above 335 K. An Arrhenius expression of $k_0 = (2.5 \pm 7.4) \times 10^{-32}$ exp[(4150 ± 1150)/T] cm^6 $molecule^{-2}$ s^{-1} was obtained for the low-pressure-limiting rate constant for the OH + MBO reaction in the presence of oxygen. Theoretical calculations of the energetics of the OH + MBO reaction suggest that the stability of the different HO−MBO adducts are similar, with predicted stabilization energies between 27.0 and 33.4 kcal mol^{-1} relative to the reactants, with OH addition to the internal carbon predicted to be 1−4 kcal mol^{-1} more stable than addition to the terminal carbon. These stabilization energies result in estimated termolecular rate constants for the OH + MBO reaction using simplified calculations based on RRKM theory that are in reasonable agreement with the experimental values.

Introduction

Methylbutenol (2-methyl-3-buten-2-ol, or MBO) is a volatile organic compound (VOC) emitted to the atmosphere by certain pine species native to North America such as lodgepole and ponderosa pine.[1] High concentrations of methylbutenol have been measured in the atmosphere at a remote site in the Colorado Mountains with daytime mixing ratios between 2 and 3 ppb, a level 5−8 times larger than those of isoprene.[2] Methylbutenol was also observed to show a strong diurnal pattern like isoprene, with a rapid increase after sunrise and a rapid decrease after sunset. Although the North American emission rate of methylbutenol is estimated to be only 3.2 Tg C per year, contributing about 4% of the total VOC flux from vegetation in North America, methylbutenol is expected to be found with high concentrations in certain regions of the atmosphere and could have a significant influence on local and regional atmospheric chemistry.[3]

Although methylbutenol can react with O_3 and NO_3,[4−6] its reaction with the hydroxyl radical (OH) is thought to be the dominant loss mechanism.[7−10] The reaction of methylbutenol with OH is believed to proceed by OH addition to the double bond to form HO−MBO adducts,[7] and studies of the reaction products suggested that OH addition to the terminal carbon accounts more than 60% of the total reaction.[11] Under atmospheric conditions, the HO−MBO adducts quickly react with O_2 to form dihydroxyalkyl peroxy radicals, which then can react with NO to form dihydroxyalkoxy radicals and NO_2. Decomposition of these dihydroxyalkoxy radicals leads to the production of HO_2 radicals and carbonyl species. Acetone, glycolaldehyde, 2-hydroxy-2-methyl-propanal, formaldehyde, and hydroxyaldehydes have been observed as some of the major products of the reaction of methylbutenol with OH:[11−14]

$$OH + (CH_3)_2C(OH)CH{=}CH_2 \rightarrow (CH_3)_2C(OH)C\cdot HCH_2OH \quad (1)$$

$$(CH_3)_2C(OH)C\cdot HCH_2OH + O_2 \rightarrow (CH_3)_2C(OH)CH(OO\cdot)CH_2OH \quad (2)$$

$$(CH_3)_2C(OH)CH(OO\cdot)CH_2OH + NO \rightarrow (CH_3)_2C(OH)CH(O\cdot)CH_2OH + NO_2 \quad (3)$$

$$(CH_3)_2C(OH)CH(O\cdot)CH_2OH \rightarrow HOCH_2CHO + (CH_3)_2C(OH)\cdot \quad (4a)$$

$$(CH_3)_2C(OH)CH(O\cdot)CH_2OH \rightarrow (CH_3)_2C(OH)CHO + \cdot CH_2OH \quad (4b)$$

$$(CH_3)_2C(OH)\cdot + O_2 \rightarrow (CH_3)_2CO + HO_2 \quad (5a)$$

$$\cdot CH_2OH + O_2 \rightarrow HCHO + HO_2 \quad (5b)$$

Recent ground-based measurements of the concentration of OH radicals in the atmosphere are generally lower than that predicted by most photochemical models[15−18] with a few measurements that were higher than predicted.[19,20] The observed discrepancies between measured and modeled concentrations of OH suggest that the current knowledge of the sinks and sources of OH radicals may be incomplete. Methylbutenol with its high abundance and reactivity can be a significant loss of atmospheric OH radicals in certain regions of the atmosphere. Therefore, an accurate knowledge of the rate constant and mechanism of the OH-initiated oxidation of methylbutenol and

* To whom correspondence should be addressed. E-mail: pstevens@indiana.edu.

10.1021/jp066286x CCC: $37.00
Published on Web 01/05/2007

other oxygenated organic compounds is essential for improving the accuracy of atmospheric chemistry models.

This paper presents the results of measurements of the rate constants for the OH + MBO reaction between 2 and 5 Torr and between 300 and 415 K using a discharge-flow system coupled with either laser-induced fluorescence detection (LIF) or resonance fluorescence (RF) detection of OH. In addition, measurements of the rate constant for the OD + MBO reaction at 5 Torr and over a similar temperature range are presented. Theoretical calculations of the stabilization energies of the individual HO−MBO adducts are used in unimolecular rate theory to predict the low-pressure-limiting rate constant for the OH + MBO reaction and the branching ratio for the initial OH addition.

Experimental Methods

The discharge-flow systems used in this study are similar to those described in detail elsewhere.[21] The main body of the flow system consists of a 100 cm long, 2.5 cm i.d. Pyrex tube connected to an aluminum detection cell. All surfaces exposed to radicals are coated with halocarbon wax (Halocarbon Corporation) to reduce the wall loss of OH. Helium (Indiana Oxygen 99.995%) was added through an MKS 1179 flow controller, and average flow velocities of approximately 10 m s^{-1} were maintained by a mechanical pump (Leybold D16B) downstream of the detection zone. The reaction zone of the flow tube was wrapped with heating tape for temperature regulation, and the reaction temperature was measured using a thermocouple inserted into the reaction zone. The pressure of the reactor is measured in the middle of the reaction zone by an MKS Baratron capacitance manometer.

OH radicals were produced either by the $F + H_2O \rightarrow OH + HF$ reaction or the $H + NO_2 \rightarrow OH + NO$ reaction. Fluorine atoms were generated by a microwave discharge of CF_4 (2% in UHP He, Matheson) in presence of He, and an excess of H_2O was injected into the flow tube 2 cm downstream of the F atom source. Hydrogen atoms were generated by a microwave discharge of H_2 (99.999% Indiana Oxygen) in the presence of He, and excess concentrations of NO_2 were injected into the flow tube 2 cm downstream of the H atom source. OD radicals were produced similarly using the $F + D_2O$ (99.9%, Cambridge Isotope Laboratories, Inc.) $\rightarrow$ OD + DF reaction.

OH radicals were detected by laser-induced fluorescence using the $A^2\Sigma^+$ ($v' = 1$) $\rightarrow$ $X^2\Pi$ ($v'' = 0$) band via $Q_1(1)$ transition near 282 nm. The excitation radiation was produced by the frequency-doubled output of a dye laser (Lambda Physik) pumped by a 3 kHz diode-pumped Nd:YAG laser (Spectra Physics). The OH A-X fluorescence near 308 nm was detected by a photomultiplier tube (Hamamatsu H 6180−01) located perpendicular to the laser radiation. A 10 nm band-pass, 20% transmissive interference filter (Esco products) centered at 308 nm was placed in front of the PMT to isolate the fluorescence from the laser scatter. The OH detection sensitivity was approximately 2×10^{-6} counts s^{-1} cm^3molecule^{-1} at a laser power of 1 mW with a background signal of approximately 7000 counts s^{-1} resulting in a minimum detectable OH concentration of approximately 2×10^7 molecules cm^{-3} (S/N = 1, 10 s integration). OD radicals were detected similarly by excitation via the $Q_1(1)$ transition near 287.4 nm. Alternatively, OH radicals were detected by resonance fluorescence using the $A^2\Sigma^+$ ($v'=0$)$\rightarrow$ $X^2\Pi$ ($v''=0$) transition near 308 nm. The excitation radiation was produced by a microwave discharge of water in the presence of helium. The system sensitivity was approximately 1×10^{-8} counts s^{-1} cm^3 molecule $^{-1}$, resulting in a minimum detectable limit of approximately 1×10^9 molecules cm^{-3} for OH (background signal = 300−400 counts s^{-1}, S/N = 1, 10 s integration).

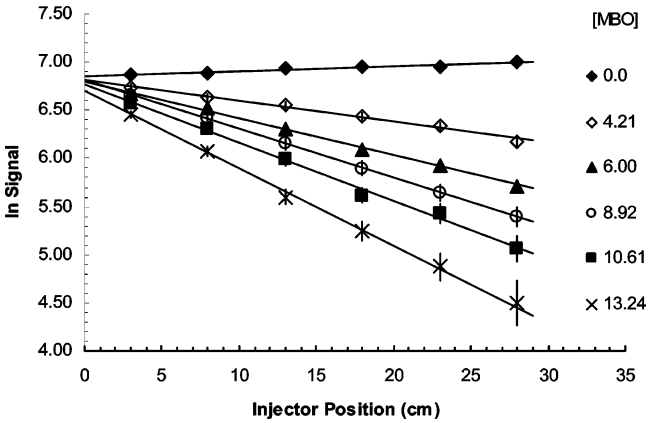

Figure 1. Sample pseudo-first-order decays of the measured OH signal for the OH + MBO reaction (5 Torr, 300 K). Methylbutenol concentrations are in 10^{11} molecules cm^{-3}. Error bars represent 2σ uncertainty.

Pseudo first-order conditions were maintained during all experiments and the OH concentrations were kept below 3×10^{11} molecules cm^{-3}. Methylbutenol (Aldrich, 99%) was purified by several freeze−pump−thaw cycles, and dilute mixtures in He were prepared by distillation. The methylbutenol was added in excess through a movable injector (3 mm o.d.) coated with halocarbon wax, and the reaction time was varied by changing the position of this injector. The concentration of methylbutenol was determined by measuring the pressure drop in a calibrated reservoir over time.

Computational Methods. Geometry optimizations for the OH + MBO reaction system were conducted using the Gaussian 03 system of programs[22] on the Indiana University IBM Power4/Power PC970 AIX Libra cluster system. The geometry of the reactants and each adduct was optimized using both Becke's three parameter hybrid method employing the LYP correction functional (B3LYP) with the 6-31G** and 6-311+G* basis sets, and using second-order Møller-Plesset perturbation theory (MP2) in conjunction with the 6-31G** and 6-311+G* basis sets. Frequencies for both reactants and products were calculated at B3LYP/6-31G** and B3LYP/6-311+G* levels of theory.

Experimental Results. Pseudo first-order decay rates (k^1_{decay}) of OH were obtained from the slope of the logarithm of the OH fluorescence signal versus reaction distance for a given concentration of methylbutenol. The first-order decay rates were corrected for axial diffusion and OH loss on the movable injector using the following equation:[23]

$$k^1 = k^1_{decay}\left(1 + \frac{k^1_{decay}D}{v^2}\right) - k_{injector} \qquad (6)$$

Here, D is the OH diffusion coefficient in He (0.145 $T^{2/3}$ P Torr cm^2 s^{-1}), v is the average flow velocity (10.0 − 14.0 m s^{-1}), and $k_{injector}$ is the loss rate of OH on the movable injector, which was measured in the absence of methylbutenol (<10 s^{-1}). A series of typical first-order decay plots for the OH + MBO reaction is shown in Figure 1.

The rate constants for the OH + MBO and the OD + MBO reactions were measured at 5 Torr between 300 and 415 K, and the results are summarized in Table 1. Additional measurements of the rate constant for the OH + MBO reaction in the presence of added oxygen as a function of temperature and

TABLE 1: Summary of Experimental Conditions and Results for the OH + MBO and OD + MBO Reactions

T (K)	[He] (10^{16} cm^{-3})	[MBO] (10^{11} cm^{-3})	no. of exp.	k^{II} (10^{-11} cm^3 molecule^{-1} s^{-1})[a]
		OH + MBO without added O_2 (5 Torr)		
300	6.8 (2 Torr)	3.3−20.2	21	5.59 ± 0.35
	8.7 (3 Torr)	5.4−20.7	16	5.38 ± 0.31
	15.9 (5 Torr)	4.3−20.0	32	5.49 ± 0.44
335	14.2	6.7−23.1	29	4.20 ± 0.45
355	13.1	6.9−23.7	27	3.06 ± 0.42
375	12.6	6.5−22.2	20	2.53 ± 0.55
395	13.1	11.1−45.7	13	2.04 ± 0.54
415	12.3	15.1−51.0	10	1.76 ± 0.34
		OD + MBO (5 Torr)		
300	16.5	4.6−18.0	33	6.61 ± 0.66
315	15.7	6.9−21.1	13	5.46 ± 0.80
325	14.9	6.9−29.2	14	4.57 ± 0.82
335	14.4	5.2−15.4	9	4.42 ± 0.57
355	13.9	7.7−22.5	8	3.47 ± 0.58
375	13.0	12.8−36.6	9	2.83 ± 0.34
392	13.0	9.5−50.0	7	1.61 ± 0.08
395	12.6	13.7−45.9	10	1.96 ± 0.62
415	12.4	12.5−42.7	9	1.80 ± 0.32
		OH + MBO with added O_2		
300	6.4 (2 Torr)	6.5−16.1	57	6.44 ± 0.42
	9.7 (3 Torr)	10.1−18.9	17	6.26 ± 0.72
	16.1 (5 Torr)	3.5−27.5	98	6.32 ± 0.27
335	7.1	5.4−19.1	11	3.48 ± 0.46
	9.9	7.0−19.5	10	3.69 ± 0.30
	14.7	5.9−17.2	18	4.40 ± 0.94
355	5.8	6.0−31.0	13	2.82 ± 0.48
	8.7	6.1−18.6	11	3.00 ± 0.64
	14.8	6.4−21.8	12	3.34 ± 0.48
375	5.4	8.7−44.6	15	1.78 ± 0.30
	8.2	11.9−39.4	13	1.94 ± 0.54
	13.8	10.1−36.5	10	2.15 ± 0.40
395	5.8	14.6−60.2	13	1.36 ± 0.18
	8.3	13.5−54.4	13	1.61 ± 0.18
	13.8	9.6−57.5	24	1.79 ± 0.16
415	5.8	18.2−73.6	12	0.93 ± 0.12
	7.9	20.1−77.1	10	0.99 ± 0.12
	13.0	16.2−64.7	12	1.33 ± 0.22

[a] Uncertainties represent 2 standard deviations.

pressure are also summarized in Table 1. Figure 2 shows example second-order plots of k^1 versus the concentration of methylbutenol for the OH + MBO reaction, the OD + MBO reaction, and the OH + MBO reaction in the presence of added O_2. For the OH + MBO reaction, a weighted linear least-squares fit of the data (based on the precision of each measurement) results in a value of $(5.49 \pm 0.44) \times 10^{-11}$ cm^3 molecule^{-1} s^{-1} for the rate constant at 300 K and 5 Torr, with the reported uncertainty representing two standard deviations from the uncertainty in the weighted fit. For the OH + MBO reaction in the presence of approximately 5−15% O_2, a weighted linear least-squares fit of the data results in a measured rate constant of $(6.32 \pm 0.27) \times 10^{-11}$ cm^3 molecule^{-1} s^{-1} at 300 K and 5 Torr. For the OD + MBO reaction, a weighted least-squares fit of the data results in a value of $(6.61 \pm 0.66) \times 10^{-11}$ cm^3 molecule^{-1} s^{-1} for the rate constant at 300 K and 5 Torr.

There have been several published measurements of the rate constant for the OH + MBO reaction. Rudich et al.[7] found a value of $(5.4 \pm 0.4) \times 10^{-11}$ cm^3 molecule^{-1} s^{-1} for the OH + MBO reaction in 100 Torr of He at 299 K, and a value of $(5.0 \pm 0.5) \times 10^{-11}$ cm^3 molecule^{-1} s^{-1} at 315 Torr and 301 K, both measured in the absence of added O_2 using a flash photolysis technique with laser-induced fluorescence detection of OH. In the presence of added O_2, they found a value of $(6.1 \pm 0.6) \times 10^{-11}$ cm^3 molecule^{-1} s^{-1} at 301 K. Imamura et al.[10] used relative rate methods and obtained a value of $(6.6 \pm 0.5) \times 10^{-11}$ cm^3 molecule^{-1} s^{-1} at 298 K and 760 Torr of air in an environmental chamber using di-*n*-butyl ether and propene as reference compounds. The room-temperature rate constants reported here are in excellent agreement with these previous measurements. The measured rate constants are also in good agreement with the reported rate constant of $(5.67 \pm 0.13) \times 10^{-11}$cm^3 molecule^{-1} s^{-1} measured by Papagni et al.[9] at 296 K and 740 Torr of air using relative rate methods with 1,3,5-trimethylbenzene as the reference compound, and the value of $(6.9 \pm 1.0) \times 10^{-11}$ cm^3 molecule^{-1} s^{-1} at 295 K and 700 Torr of air reported by Ferronato et al.[13] using relative rate techniques in an environmental chamber using ethylene and propylene as the reference compounds, but are larger than the value of $(3.9 \pm 1.2) \times 10^{-11}$ cm^3 molecule^{-1} s^{-1} reported by Fantechi et al. at 298 K and 740 Torr of air using relative rate techniques with isoprene and propene as the reference compounds.[8] The results reported here for the measurements of the rate constant for the OD + MBO reaction are also in excellent agreement with the results of Rudich et al., who report a value of $(6.2 \pm 0.5) \times 10^{-11}$ cm^3 molecule^{-1} s^{-1} at 300 K and 95 Torr.[7]

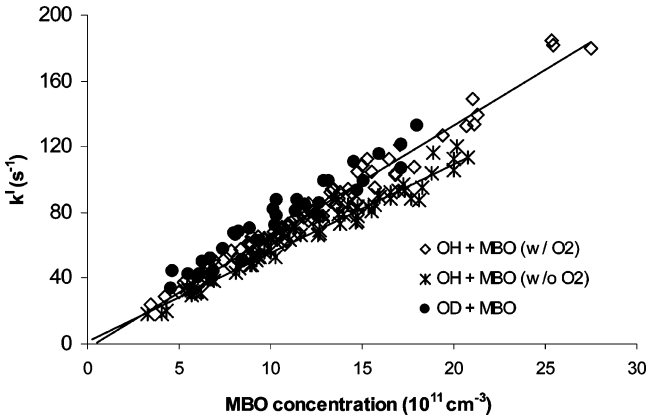

Figure 2. Second-order plot of k^1 versus [MBO] for the OH + MBO and OD + MBO reactions at 5 Torr and 300 K. Solid lines represent fits to the OH + MBO with added O_2 and OD + MBO reactions, and the OH + MBO without added O_2.

The measured rate constant for the OH + MBO reaction in the absence of O_2 is about 15% lower than that measured at room temperature for both the OH + MBO reaction in the presence of added O_2 and the OD + MBO reaction, similar to that observed by Rudich et al., who also observed the appearance of OH radicals from the OD + MBO reaction.[7] Rudich et al. suggested that the lower observed rate constant for the OH + MBO reaction in the absence of oxygen was due to the elimination of the alcohol OH group from the adduct formed following OH addition to the double bond of methylbutenol:

$$(CH_3)_2C(OH)CH-C(OH)H_2 \rightarrow OH + (CH_3)_2C{=}CH-C(OH)H_2 \quad (7)$$

In the absence of O_2, a fraction of the HO−MBO adducts formed by OH addition to methylbutenol may decompose to eliminate the alcohol OH group. As a result, the rate constant obtained by measuring the loss of OH radicals would appear to be lower than the actual value due to the reappearance of OH. Adding oxygen presumably prevents the elimination of the alcohol OH group from the HO−MBO adducts by rapidly forming more stable dihydroxyalkyl peroxy radicals.[7]

To further test this effect, we varied the percentage of O_2 added from 0 to 15%, and the oxygen dependence of the rate constant is shown in Figure 3. As can be seen from this Figure,

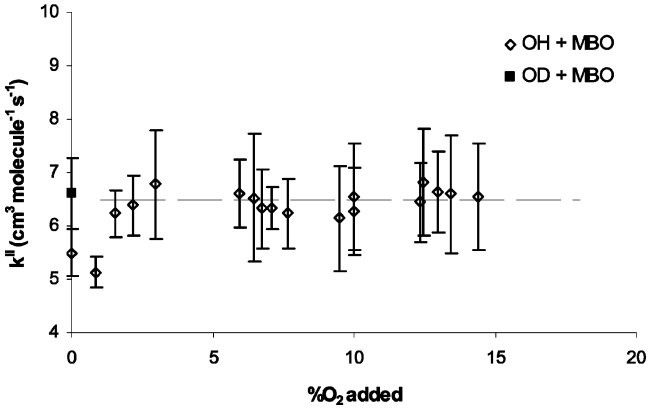

Figure 3. Measured rate constants for the OH + MBO and OD + MBO reactions at 5 Torr and 300 K as a function of added O_2. Uncertainties represent 2 standard deviations. Dashed line is the average value of all measurements with more than 5% added O_2.

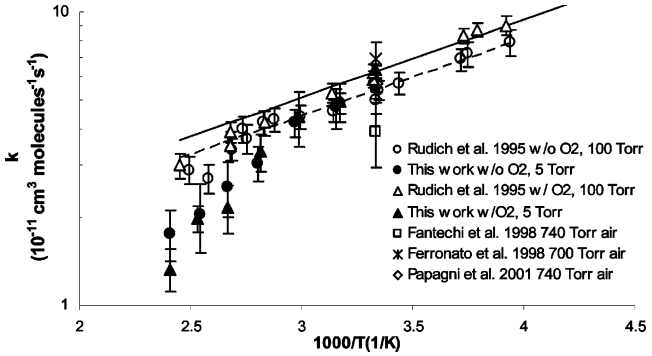

Figure 4. Arrhenius plot for the reaction of OH with MBO with and without added O_2. Solid line is the recommended Arrhenius expression of Rudich et al. for the reaction in the presence of O_2 over the temperature range 230−360 K, whereas the dashed line is the recommended expression in the absence of O_2 over the temperature range 254−320 K (ref 7).

the rate constant for the OH + MBO reaction is independent of the amount oxygen added at concentrations higher than approximately 4%, and approaches the rate constant for the OD + MBO reaction. This is consistent with the results of Rudich et al., who found that at 100 Torr the formation of OH in the reaction of OH with MBO was completely suppressed by 7 Torr of O_2.[7] This agreement suggests that the elimination of the alcohol OH group from the excited adduct was not enhanced significantly under the low-pressure conditions of these experiments. Unfortunately, OH radical impurities produced from the microwave discharge interfered with measurements of the concentration of OH produced from the OD + MBO reaction.

The measured rate constants as a function of temperature for the OH + MBO reaction, both in the presence and absence of O_2 at 5 Torr are shown in Figure 4, together with previous measurements under similar conditions. The rate constant for this reaction displays a negative temperature dependence consistent with an OH addition mechanism. As can be seen from this Figure, our 5 Torr results both in the presence and absence of added O_2 are in agreement with the results of Rudich et al. measured near 100 Torr with and without added oxygen for temperatures below 335 K.[7] However, above 335 K, the measured low-pressure rate constants are significantly smaller than those measured at higher pressures. Figure 5 shows a plot of the temperature dependence for the OD + MBO reaction at 5 Torr. As observed for the OH + MBO reaction, the results from this study for temperatures below 335 K are similar to those measured by Rudich et al. at higher pressures[7] but become

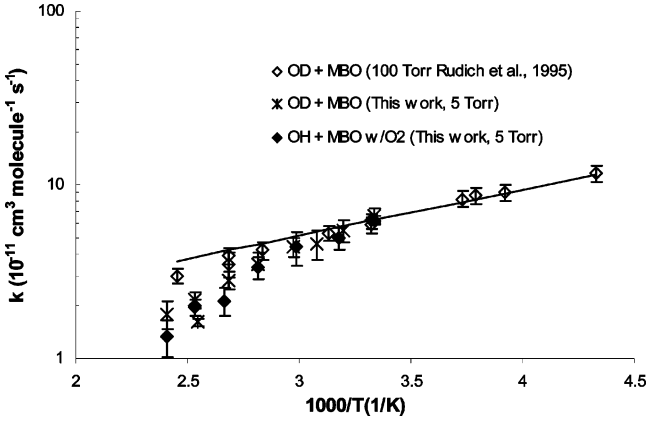

Figure 5. Arrhenius plot for the OD + MBO reaction and the OH + MBO reaction with added O_2 at 5 Torr. Solid line is the recommended Arrhenius expression of Rudich et al. over the temperature range 230−360 K (ref 7).

smaller than the higher pressure measurements as the temperature increases.

As shown in Figure 5, the measured rate constants for the OH + MBO reaction in the presence of O_2 agree well with the values obtained for the OD + MBO reaction within the experimental uncertainty over the temperature range of this study, suggesting that enough oxygen was added to hinder elimination of the alcohol OH group even at high temperatures. These results imply that the decrease in the rate constant at low pressure and high temperature compared to the higher pressure results is not solely due to an increase in the rate of alcohol OH elimination in the HO−MBO adduct, but is likely due to an additional increased rate of thermal dissociation of the added OH in the excited adduct.

The agreement between the rate constants measured at room temperature and low pressures (2, 3, and 5 Torr) with those measured at higher pressures suggests that the OH + MBO reaction is still at its high-pressure limit at room temperature and at pressures as low as 2 Torr. This suggests that the excess energy due to the addition of OH to the double bond of methylbutenol is easily distributed through the large number of available vibrational degrees of freedom, and the excited adducts are stabilized quickly with a minimal necessary number of third body collisions. However, at higher temperatures the rate of thermal dissociation of the HO−MBO adducts increases and begins to compete with the rate of stabilization, leading to an observed falloff of the rate constant at low pressure.

This falloff of the rate constant at higher temperatures and low pressures is shown in Figure 6, and is similar to that observed at low pressure and high temperatures for the reaction of OH with other unsaturated molecules such as isoprene,[21] methyl vinyl ketone,[24] and α- and β-pinene,[25] and is consistent with a Lindemann−Hinshelwood mechanism:

$$\mathrm{OH} + \mathrm{MBO} \rightarrow \mathrm{HO{-}MBO^*} \quad (8)$$

$$\mathrm{HO{-}MBO^*} \rightarrow \mathrm{OH} + \mathrm{MBO} \quad (9)$$

$$\mathrm{HO{-}MBO^*} + \mathrm{M} \rightarrow \mathrm{HO{-}MBO} + \mathrm{M^*} \quad (10)$$

According to Troe, the falloff of the bimolecular rate constants with pressure can be predicted by the following equation:[26,27]

$$k^{\mathrm{II}} = \left(\frac{k_0(T)[M]}{1 + \frac{k_0(T)[M]}{k_\infty(T)}}\right) F_c^{\left(\frac{1}{1+[\log(k_0(T)[M]/k_\infty(T))]^2}\right)} \quad (11)$$

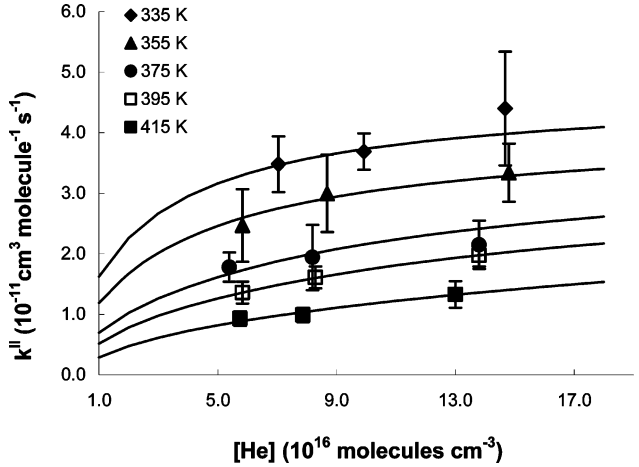

Figure 6. Plot of the second-order rate constant k^{II} versus the concentration of He at different temperatures for the OH + MBO reaction in the presence of added O_2. The solid lines represent the weighted least-squares fits to the data using eq 11 and assuming $k_\infty = 8.2 \times 10^{-12}$ e$^{(610/T)}$ cm^3 molecule^{-1} s^{-1} (ref 7).

Here, k_0 is the termolecular rate constant at the low-pressure limit, k_∞ is the rate constant at the high-pressure limit, and F_c is the collisional broadening factor. Due to the limited pressure range of this study, both k_0 and k_∞ cannot be determined accurately. However, if the 100 Torr value of $k = 8.2 \times 10^{-12}$ e $^{(610/T)}$ cm^3 molecule^{-1} s^{-1} reported by Rudich et al.[7] is used for k_∞ and a value of 0.6 is assumed for F_c,[26,27] a weighted nonlinear least-squares fit of the data shown in Figure 6 to eq 11 for each temperature results in the derived k_0 values listed in Table 2 and shown in Figure 7, with the reported error representing twice the standard error from the weighted fit. The experimental data at 335 K are more consistent with a value of 0.7 for F_c, similar to that observed for the OH + isoprene reaction.[21] This is not surprising, as collisional broadening is expected to increase with decreasing temperature.[28]

A weighted linear least-squares fit of the derived k_0 for the OH + MBO reaction versus inverse temperature yields the following Arrhenius expression for the low-pressure-limiting rate constant, where the uncertainties represent two standard errors from the fit:

$$k_0 = (2.5 \pm 7.4) \times 10^{-32} \exp[(4150 \pm 1150)/T] \text{ cm}^6 \text{ molecule}^{-2} \text{ s}^{-1} \quad (12)$$

The negative activation energy of the low-pressure-limiting rate constant for the OH + MBO reaction is consistent with an OH addition mechanism, similar to that found for the reaction of OH with other unsaturated VOCs, as shown in Figure 7. As can be seen from this Figure, the negative activation energy at the low-pressure limit for this reaction ($E_a/R = -4150$ K) appears to be greater than those for the reaction of OH with isoprene,[21] ethylene,[21] and methyl vinyl ketone.[24] However, the overall errors in the derived k_0 values reported in Table 2 are likely to be significantly larger than the statistical errors reported here, as the fit of the data to eq 11 is not highly constrained due to the limited number of measurements and their corresponding uncertainties, in addition to uncertainties associated with the assumed values of k_∞ and F_c. As a result, it is possible that the derived values of k_0 and the negative activation energy reported here may not be significantly different than that for the OH + isoprene reaction or the OH + methyl vinyl ketone reaction, which were derived in a similar fashion.[21,24]

Whereas there is a significant difference in the measured rate constant for the OH + MBO reaction without added O_2 at room temperature compared to the OD + MBO reaction and the OH + MBO reaction in the presence of added O_2, there does not appear to be a significant difference in the measured rate constants at higher temperatures (Figure 4). This suggests that at elevated temperatures the rate of thermal decomposition of the HO−MBO adducts (reaction 5) competes with the rate at which the alcohol OH is eliminated. Similar results at elevated temperatures and at 100 Torr were reported by Rudich et al., who also observed non-Arrhenius behavior above 320 K.[7] These authors suggested that thermal decomposition of the HO−MBO adduct may be responsible for this non-Arrhenius behavior, similar to that observed for the reaction of OH with aromatic hydrocarbons.[7] However, a close examination of the measurements suggests the possibility that at higher temperatures the rate constants for the OH + MBO in the absence of added O_2 are larger than those measured in the presence of added O_2 (Figure 4), in contrast to the results at low temperature, perhaps indicating a more complicated mechanism for OH elimination. Additional studies at higher temperatures and pressures are still needed to resolve the temperature dependence of this reaction and perhaps observe a thermal equilibrium between OH, methylbutenol and the HO−MBO adduct, and to provide additional insight into the mechanism of the OH elimination pathway.

Discussion

To gain insight into the mechanism of the OH + MBO reaction, the ab initio relative stabilities of the HO−MBO adducts were calculated and used to estimate the low-pressure-limiting rate constants for the OH + MBO → adducts reaction. At the low-pressure limit, the overall rate constant for the reaction is limited by the rate of intermolecular energy transfer which is dependent on the relative stability of the adducts.[29] The theoretical results were used in simplified equations based on RRKM theory to estimate the second-order rate constant for the unimolecular dissociation of the HO−MBO adducts,[26,27,29,30] and the resulting rate constants were then used to estimate the reverse third-order association rate constant through the equilibrium constant for the OH + MBO reaction, assuming that the barrier to formation of the adducts is negligible.[31] These estimated OH + MBO association rate constants were then compared to the observed values to determine whether the stability and structure of the adducts are consistent with the observed negative activation energy. In addition, the structure and energies of the OH-elimination products and peroxy radicals produced after subsequent reaction with O_2 were calculated to gain insight to the nature of the potential energy surface for this reaction.

Ab initio Calculations. Figure 8 illustrates the optimized geometries for the OH + MBO reaction. Initial geometries for the reactants, HO−MBO adducts and products were optimized at the B3LYP/6-31G** level of theory, whereas the reactants and the HO−MBO adducts were further optimized at the B3LYP/6-311+G*, MP2/6-31G** and the MP2/6-311+G* levels of theory. The geometries optimized at the B3LYP level of theory for each HO−MBO adduct were consistent with those optimized at the MP2 level of theory.

Addition of OH to methylbutenol can occur either at the terminal carbon (adduct 1) or the internal carbon (adduct 2) of the double bond, resulting in adducts with both cis and trans structures relative to the OH groups. The resulting cis isomers are approximately 2−3 kcal/mol more stable than the corresponding trans isomers, as the cis isomers benefit from additional stability due to hydrogen bonding between the OH

TABLE 2: Experimental and Theoretical Values of k_0 for the OH + MBO Reaction

T (K)	k_0 (experiment) (10^{-28} cm^6 molecule^{-2} s^{-1})[a]	k_{rec}^{wc} (B3LYP/6-311+G*) ($\beta = 0.01$) (10^{-28} cm^6 molecule^{-2} s^{-1})	k_{rec}^{wc} (MP2/6-311+G*) ($\beta = 0.0005$) (10^{-28} cm^6 molecule^{-2} s^{-1})
335	42.6 ± 9.3	46	44
355	34.4 ± 5.8	30	28
375	14.1 ± 4.1	19	18
395	9.3 ± 0.1	12	11
415	4.3 ± 0.5	8	7

[a] Experimental uncertainties represent 2 standard deviations.

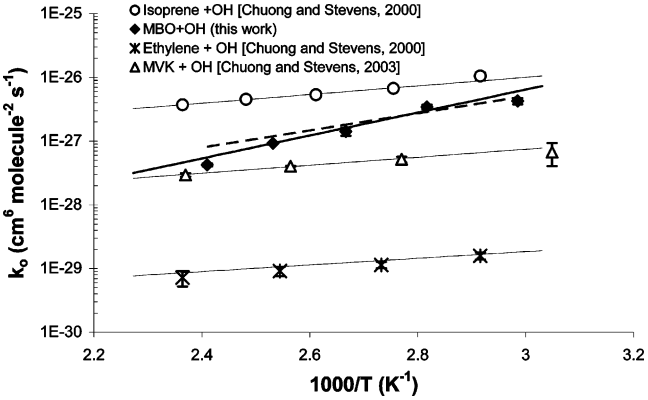

Figure 7. Arrhenius plot of the low-pressure-limiting rate constants for the reaction of OH with several alkenes. k_0 values for the OH + MBO reaction in the presence of added O_2 were derived from the Troe equation assuming $k_\infty = 8.2 \times 10^{-12}$ e $^{(610/T)}$ cm^3 molecule^{-1}s^{-1}. Dashed line is the calculated low-pressure-limiting rate constant for the OH + MBO reaction using the ab initio stabilization energies (see text).

groups (Figure 8). There are also two conformations for each of the cis isomers depending on the nature of the hydrogen bond between the OH groups, either with the hydrogen bonded interaction between the hydrogen of the alcohol OH with the lone pair electrons of the added OH (adducts 1 and 2) or with the hydrogen bonded interaction between the hydrogen of the added OH with the lone pair electrons of the alcohol OH. The difference in the relative energies for these different hydrogen-bonded conformations is less than 1 kcal mol^{-1}. For simplicity, only adducts 1 and 2 were considered in these calculations.

At the B3LYP/6-311+G* level of theory, the C−C bond length between carbons 3 and 4 in adduct 1 is approximately 0.153 Å longer relative to methylbutenol, reflecting an increased σ character of the C−C bond as electron density in the Π bond is transferred to the newly formed C−O bond. A similar lengthening of the C−C bond between carbons 3 and 4 (0.151 Å) is also predicted upon addition of OH to the 3 carbon of methylbutenol (adduct 2). The remaining bonds in both adduct 1 and adduct 2 are similar in length to the corresponding bonds in methylbutenol, suggesting that the unpaired electron is localized on carbon 3 for adduct 1 and carbon 4 for adduct 2.

The total energies along with the spin eigenvalues (S^2) associated with the optimized geometries for OH, methylbutenol, and each HO−MBO adduct for each level of theory are listed in Table 3 with the zero point energy correction (ZPE). Contamination of the unrestricted wave functions from higher spin states is minimal for OH and adducts 1 and 2, as the expected value for S^2 for each of these species is close to the exact value of 0.750 for a pure doublet. Table 4 shows the B3LYP/6-31G** and B3LYP/6-311+G* frequencies for OH, methylbutenol, adduct 1 and adduct 2. The absence of any imaginary frequencies confirms that the optimized geometry for each adduct is at a local minimum on the potential energy surface.

Table 5 lists the relative energetics computed at each level of theory for the OH + MBO reaction, and are illustrated in Figure 8. At the B3LYP/6-31G** + ZPE level of theory, the stability of the HO−MBO adducts are very similar, with addition to the internal carbon (adduct 2) predicted to be slightly more stable (31.4 kcal mol^{-1}) than addition to the terminal carbon (30.1 kcal mol^{-1}) relative to the reactants. At the B3LYP/6-311+G* + ZPE level of theory, the difference in stability between these two adducts is also similar, with calculated stabilization energies of 28.1 and 27.0 kcal mol^{-1} for adducts 2 and 1, respectively. This order of stability is independent of the level theory of the calculation, as the results at the MP2/6-31G** and MP2/6-311+G* levels of theory are similar. At the MP2/6-311+G* + ZPE level of theory (using the B3LYP/6-311+G* frequencies), adduct 2 is predicted to be approximately 4 kcal mole^{-1}more stable than adduct 1, with adduct 2 and 1 predicted to be 33.4 and 29.3 kcal mol^{-1} more stable than the OH and methylbutenol reactants. This is in contrast to the conclusions of Rudich et al. who proposed that the addition of OH to the terminal carbon should be more stable, as the resulting radical is localized on the more substituted carbon.[7] The decrease in stability for addition of OH to the terminal carbon may be due to increased repulsion between the unpaired electron localized on carbon 3 with the lone pairs of the added OH group. The calculated HOMO for adduct 1 has significant p-orbital character on C3 perpendicular to the C2−C3-C4 plane, overlapping with the electron pairs of the added OH oxygen, whereas the calculated HOMO of adduct 2 has significant p-orbital character on the terminal C4 carbon, which does not overlap with the added OH lone pairs.

In addition to the stabilization energy of the HO−MBO adducts relative to the OH and methylbutenol reactants, the energy relative to alcohol OH elimination from adduct 1 leading to the formation of 3-methyl-2-buten-1-ol (3MBO) was also calculated. At the B3LYP/6-31G** + ZPE level of theory, the dissociation energy was found to be approximately 31.8 kcal mol^{-1}, which is approximately 1−2 kcal mol^{-1} greater than dissociation to the OH + MBO reactants at the same level of theory (Figure 8). Elimination of the alcohol OH group from adduct 2 leading to the formation of 2,2-dimethyl-cyclopropanol (DMPO) is less favorable, with a calculated minimum dissociation energy of 38.9 kcal mol^{-1} at the B3LYP/6-31G** +ZPE level of theory, which is approximately 7 kcal mol^{-1} greater than dissociation back to reactants. Reaction of each adduct with O_2 leads to the formation of peroxy radicals which are calculated to be approximately 29.1 and 28.5 kcal mol^{-1} more stable than adducts 2 and 1, respectively, at the B3LYP/6-31G** + ZPE level of theory (Figure 8). Similar to the individual adducts, the peroxy radical resulting from reaction of adduct 2 with O_2

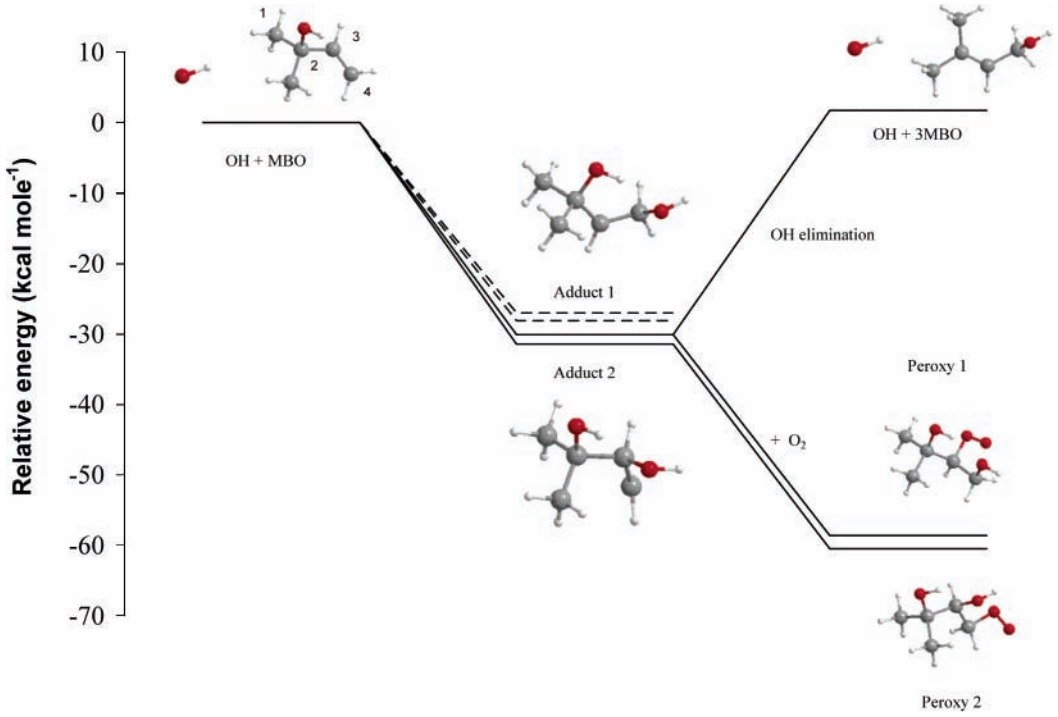

Figure 8. Schematic potential energy surface for the OH + MBO reaction. Solid lines represent the relative energies calculated at the B3LYP/6-31G** level of theory, while the dashed lines represent the relative energies at the B3LYP/6-311+G* level of theory.

TABLE 3: Total Energy (Hartrees), Spin Eigenvalues, and Zero Point Energy (Hartrees) for the OH + MBO → Reaction

species	B3LYP/6-31G**	S^2	ZPE	B3LYP/6-311+G*	S^2	ZPE	MP2/6-31G**	S^2	MP2/6-311+G*	S^2
OH	−75.72848	0.752	0.00842	−75.75488	0.752	0.00833	−75.53209	0.755	−75.56489	0.756
MBO	−271.76504	0	0.14115	−271.81906	0	0.14056	−270.90644	0	−270.94268	0
adduct 1	−347.54775	0.754	0.15584	−347.62331	0.754	0.15520	−346.49327	0.763	−346.56052	0.764
adduct 2	−347.54863	0.754	0.15460	−347.62381	0.754	0.15391	−346.49727	0.763	−346.56575	0.763
3MBO	−271.76238	0	0.14124							
DMPO	−271.75387	0	0.14192							
O_2	−150.32004	2.007	0.00378							
peroxy 1	−497.91959	0.753	0.16595							
peroxy 2	−497.92238	0.753	0.16579							

(peroxy 2) is predicted to be slightly more stable than the peroxy radical resulting from reaction of O_2 with adduct 1 (peroxy 1), with calculated stabilization energies of 58.6 and 60.5 kcal mol^{-1} for peroxy 1 and 2 respectively at the B3LYP/6-31G** + ZPE level of theory. Although the elimination of the alcohol OH from adduct 1 has a similar dissociation energy compared to reformation of the reactants, these results suggest that direct dissociation of the alcohol OH may not be energetically favorable, and that the observed elimination of the alcohol OH may occur through a more complex mechanism.[7] Additional experimental and theoretical studies are needed to determine the mechanism of the OH-elimination pathway.

Calculation of the Low-Pressure-Limiting Rate Constant. The strong collision dissociation rate constant at the low-pressure limit can be expressed as:[26,27,30]

$$k_{\text{diss}}^{\text{sc}} = Z_{\text{LJ}} \frac{\rho(E_0)RT}{Q_{\text{vib}}} \exp\left(\frac{-E_0}{RT}\right) F_{\text{E}} F_{\text{anh}} F_{\text{rot}} F_{\text{corr}} \qquad (13)$$

Here, Z_{LJ} is the Lennard-Jones collision frequency, $\rho(E_0)$ is the density of states at the critical energy E_0, Q_{vib} is the vibrational partition function, and F_{E}, F_{anh}, and F_{rot} are correction terms for the energy dependence of the density of states, anharmonicity, and rotation. F_{corr} is a correction factor to account for coupling between the various degrees of freedom, and is assumed to be unity, which neglects the coupling between various vibrational and rotational degrees of freedom.[26] The strong collision association rate constant can then be obtained from the calculated equilibrium constant:

$$k_{\text{rec}}^{\text{sc}} = \frac{k_{\text{diss}}^{\text{sc}}}{K_{\text{eq}}} \qquad (14)$$

The strong collision association rate constant represents an upper limit to the observed rate constant and is multiplied by a collisional deactivation efficiency β_c to obtain the weak collision rate constant, $k_{\text{rec}}^{\text{wc}}$, which can be compared to experiment.[27,30]

The second-order rate of dissociation of the HO−MBO adducts at low pressure will depend on the rate of energization of the adducts above the dissociation threshold, E_0. For these calculations, the relative stabilization energy of each adduct at either the B3LYP/6-311+G* +ZPE or the MP2/6-311+G* level of theory was used for E_0, assuming that the barrier to dissociation is negligible. Z_{LJ} was calculated following Troe,[26] and the density of states at the critical energy, $\rho(E_0)$, was calculated using the Whitten-Rabinovitch approximation.[32] The vibrational partition function (Q_{vib}) for each adduct was calculated using the vibrational frequencies calculated at the B3LYP/6-311+G* level of theory. The correction terms F_{E}, F_{anh}, and F_{rot} were calculated following Troe[26,27] and Patrick and Golden.[30] The equilibrium constant K_{eq} for the reaction was calculated based on the B3LYP/6-311+G* +ZPE or MP2/6-

TABLE 4: Calculated Frequencies for the OH + MBO → Adduct Reaction

species	B3LYP/6-31G** frequencies (cm^{-1})	B3LYP/6-311+G* frequencies (cm^{-1})
OH	3694	3654
MBO	3798, 3240, 3162, 3145, 3138, 3134, 3129, 3115, 3054, 3045, 1722, 1525, 1515, 1501, 1494, 1461, 1426, 1410, 1362, 1326, 1285, 1202, 1141, 1058, 1043, 1016, 962, 950, 938, 902, 731, 704, 532, 444, 400, 372, 350, 323, 289, 278, 239, 99	3763, 3215, 3140, 3128, 3116, 3113, 3108, 3095, 3042, 3033, 1700, 1528, 1518, 1504, 1497, 1459, 1427, 1411, 1357, 1328, 1280, 1189, 1139, 1059, 1039, 1019, 956, 947, 941, 891, 728, 703, 533, 442, 400, 372, 332, 327, 293, 281, 241, 105
adduct 1	3793, 3704, 3193, 3133, 3128, 3124, 3115, 3049, 3048, 3040, 2976, 1521, 1512, 1509, 1498, 1490, 1451, 1426, 1422, 1398, 1373, 1275, 1252, 1219, 1193, 1132, 1092, 1018, 1011, 965, 956, 926, 882, 750, 625, 601, 524, 447, 407, 380, 341, 305, 281, 268, 234, 230, 144, 39	3763, 3691, 3175, 3112, 3108, 3103, 3094, 3053, 3036, 3028, 2976, 1523, 1513, 1508, 1499, 1491, 1443, 1425, 1416, 1400, 1370, 1276, 1245, 1215, 1188, 1130, 1094, 1023, 1012, 953, 935, 927, 878, 745, 620, 562, 527, 444, 408, 384, 336, 305, 286, 268, 235, 226, 133, 44
adduct 2	3826, 3768, 3274, 3164, 3138, 3135, 3127, 3124, 3054, 3049, 2989, 1523, 1513, 1500, 1494, 1467, 1434, 1412, 1390, 1383, 1336, 1275, 1218, 1189, 1153, 1110, 1082, 1008, 987, 941, 918, 868, 737, 577, 548, 511, 477, 442, 418, 357, 347, 298, 265, 255, 238, 227, 204, 109	3794, 3743, 3250, 3143, 3117, 3114, 3107, 3102, 3043, 3037, 3002, 1526, 1516, 1503, 1497, 1462, 1432, 1412, 1384, 1378, 1340, 1271, 1204, 1186, 1146, 1104, 1068, 1010, 980, 943, 912, 860, 734, 579, 553, 508, 460, 441, 418, 356, 342, 295, 267, 258, 238, 225, 199, 104

TABLE 5: Relative Energetics (kcal mol^{-1}) for the OH + MBO Reaction

level of theory	adduct 1	adduct 2
B3LYP/6-31G**	−34.0	−34.6
B3LYP/6-31G** + ZPE	−30.1	−31.4
B3LYP/6-311+G*	−30.0	−31.3
B3LYP/6-311+G* + ZPE	−27.0	−28.1
MP2/6-31G**	−34.4	−36.9
MP2/6-31G** + ZPE[a]	−30.4	−33.7
MP2/6-311+G*	−33.2	−36.5
MP2/6-311+G* + ZPE[b]	−29.3	−33.4

[a] Using B3LYP/6-31G** frequencies. [b] Using B3LYP/6-311+G* frequencies.

311+G* +ZPE results for the adducts and the reactants. The weak-collision association rate constant, k_{rec}^{wc} was obtained by multiplying the strong-collision association rate constant, k_{rec}^{sc} (from eq 14), by a collisional deactivation efficiency, β_c, which is derived by comparison with the experimental values.[30]

The values for each parameter in eq 13 were calculated for each adduct for both the B3LYP/6-311+G* + ZPE and MP2/6-311+G* +ZPE stabilization energies in order to compare the calculated $k_{rec,0}^{wc}$ with the experimental measurements of the low-pressure-limiting rate constant for the OH + MBO reaction. The detailed results for each adduct are summarized in Tables 6 and 7, and the overall results for both adducts are compared to the experimental values in Table 2 and Figure 7.

Using the B3LYP/6-311+G* + ZPE calculated stabilization energies for each adduct for the critical energy, the predicted values for the overall termolecular rate constant for the OH + MBO reaction, which is the sum of the rate constant for formation of each adduct, are in reasonable agreement with the experimental values using a collisional deactivation efficiency of 0.01 (Table 2). This empirically derived collisional deactivation efficiency is smaller than typical values of 0.1−0.5, and is probably due to incorrectly assuming that F_{corr}, the correction factor to account for coupling between the various degrees of freedom, is equal to unity.[30] If the MP2/6-311+G* calculated stabilization energies are used for each adduct, a collisional deactivation efficiency of 0.0005 is needed to bring the calculated overall termolecular rate constant into agreement with experiment (Table 2). If a typical collisional deactivation efficiency (β_c) of 0.1 is used in these calculations,[30] a stabilization energy of approximately 23.5 kcal mol^{-1} for both adducts 1 and 2 is required to bring the calculated termolecular rate constants into agreement with experiment.

Although there is considerable uncertainty associated with the experimentally derived values of k_0 and their temperature dependence, these simplified calculations of the low-pressure-limiting rate constant are able to reasonably reproduce the observed negative activation energy for the OH + MBO reaction compared to the OH + isoprene reaction (Figure 7). The larger negative activation energy for the OH + MBO reaction in these calculations is likely due in part to the additional low-frequency vibrations in both methylbutenol and the adducts contributing to a larger temperature dependence of the corresponding vibrational partition functions. This leads to a greater difference between the temperature dependences of k_{diss} and K_{eq} in eq 14 relative to the OH + isoprene reaction.[31] However, more detailed calculations of the rate constants for this reaction as a function of temperature are needed to confirm these results.

Although the B3LYP/6-311+G* + ZPE calculated energies predict that addition to the internal carbon (adduct 2) is slightly more stable than addition to the terminal carbon (adduct 1), the calculated low-pressure-limiting rate constants using these energies results in a predicted yield of approximately 70% for addition of OH to the terminal carbon between 335 and 415 K. The calculated yield for adduct 1 is higher because the contribution of several low-frequency vibrations in adduct 1 leads to a larger calculated vibrational partition function that reduces the rate of dissociation of adduct 1 relative to adduct 2 in eq 13 (Tables 6 and 7). These results are consistent with previous measurements of the product yields of acetone and glycoaldehyde (reaction 5b) of 0.58 ± 0.04 and 0.61 ± 0.09, respectively, suggesting preferential addition of OH to the terminal carbon.[11,14]

In contrast, if the MP2/6-311+G* +ZPE calculated stabilization energies are used for adducts 1 and 2, the calculations of the low-pressure-limiting rate constant suggest that addition to the internal carbon should be preferred, with a calculated yield of approximately 86% between 335 and 415 K. This is the result of the greater difference in the relative stability between adducts 1 and 2 leading to larger dissociation rate constants for adduct 1 relative to adduct 2 even with the larger calculated vibrational partition functions for adduct 1 (Tables 6 and 7). These results are in contrast to the suggested preference of OH addition based on product studies described above.[11,14]

However, these calculated results at low pressure may not be applicable to the overall yield of each adduct under atmospheric conditions. Recent experimental and theoretical studies suggest that the negative activation energy observed at the high-pressure limit for the OH addition to alkenes is likely due to the reversible formation of a prereactive complex through an initial transition state, followed by an irreversible reaction

TABLE 6: Contributing Factors to the Calculation of the Strong Collision Dissociation and Recombination Rate Constants for the OH + MBO → Adduct 1 Reaction Using the B3LYP/6-311+G* Calculated Stabilization Energy of 27.0 kcal mol^{-1} (and the MP2/6-311+G* Caclulated Enegy of 29.3 kcal mol^{-1})

T (K)	Z_{LJ} ($cm^3 mol^{-1} s^{-1}$)	$\rho(E_0)$ ($\times 10^9$)	Q_{vib}	F_E F_{anh} F_{rot}	k_{diss}^{sc} (cm^3 molecule^{-1} s^{-1})	K_{eq} (molecule cm^{-3})	k_{rec}^{sc} (cm^6 molecule^{-2} s^{-1})
335	3.7×10^{-10}	1.2 (4.7)	350	1.5 (1.4) 1.1 (1.1) 4.2 (4.4)	5.5×10^{-17} (7.3×10^{-18})	1.7×10^{8} (6.0×10^{6})	3.2×10^{-25} (1.2×10^{-24})
355	3.8×10^{-10}	1.2 (4.7)	550	1.5 (1.5) 1.1 (1.1) 4.0 (4.1)	3.5×10^{-16} (5.7×10^{-17})	1.7×10^{9} (7.4×10^{7})	2.1×10^{-25} (7.7×10^{-25})
375	3.8×10^{-10}	1.2 (4.7)	855	1.5 (1.5) 1.1 (1.1) 3.7 (3.8)	1.8×10^{-15} (3.4×10^{-16})	1.4×10^{10} (7.0×10^{8})	1.3×10^{-25} (4.9×10^{-25})
395	3.9×10^{-10}	1.2 (4.7)	1340	1.6 (1.6) 1.1 (1.1) 3.5 (3.6)	7.4×10^{-15} (1.6×10^{-15})	8.9×10^{10} (5.2×10^{9})	8.4×10^{-26} (3.1×10^{-25})
415	3.9×10^{-10}	1.2 (4.7)	2090	1.6 (1.6) 1.1 (1.1) 3.3 (3.4)	2.6×10^{-14} (6.5×10^{-15})	4.8×10^{11} (3.2×10^{10})	5.4×10^{-26} (2.0×10^{-25})

TABLE 7: Contributing Factors to the Calculation of the Strong Collision Dissociation and Recombination Rate Constants for the OH + MBO → Adduct 2 Reaction Using the B3LYP/6-311+G* Calculated Stabilization Energy of 28.1 kcal mol^{-1} (and the MP2/6-311+G* Calculated Energy of 33.4 kcal mol^{-1})

T (K)	Z_{LJ} ($cm^3 mol^{-1} s^{-1}$)	$\rho(E_0)$ ($\times 10^9$)	Q_{vib}	F_E F_{anh} F_{rot}	k_{diss}^{sc} (cm^3 molecule^{-1} s^{-1})	K_{eq} (molecule cm^{-3})	k_{rec}^{sc} (cm^6 molecule^{-2} s^{-1})
335	3.7×10^{-10}	6.1	160	1.5 (1.4) 1.1 (1.1) 4.2 (4.7)	9.2×10^{-17} (2.0×10^{-19})	6.4×10^{8} (2.7×10^{4})	1.4×10^{-25} (7.6×10^{-24})
355	3.8×10^{-10}	6.1	260	1.5 (1.4) 1.1 (1.1) 3.9 (4.4)	5.7×10^{-16} (2.2×10^{-18})	6.3×10^{9} (4.7×10^{5})	9.1×10^{-26} (4.8×10^{-24})
375	3.8×10^{-10}	6.1	410	1.5 (1.5) 1.1 (1.1) 3.6 (4.1)	2.8×10^{-15} (1.8×10^{-17})	4.8×10^{10} (6×10^{6})	5.8×10^{-26} (3.0×10^{-24})
395	3.9×10^{-10}	6.1	650	1.6 (1.5) 1.1 (1.1) 3.4 (3.8)	1.1×10^{-14} (1.1×10^{-16})	3×10^{11} (5.9×10^{6})	3.7×10^{-26} (1.9×10^{-24})
415	3.9×10^{-10}	6.1	1031	1.6 (1.6) 1.1 (1.1) 3.2 (3.6)	3.8×10^{-14} (5.7×10^{-16})	1.6×10^{12} (4.6×10^{8})	2.4×10^{-26} (1.2×10^{-24})

though a second transition state that is lower in energy than the reactants.[33−35] As a result, the overall yield at atmospheric pressure may depend on the structure and energetics of the transition states and intermediate complexes, rather than the stability of the individual adducts.

Conclusions

The measured rate constants for the reaction of OH with methylbutenol at 2, 3, and 5 Torr and room temperature are in good agreement with those obtained at higher pressures, suggesting that the reaction is at its high-pressure limit at room temperature and 2 Torr. However, the rate constants begin to show a pressure dependence at temperatures above 335 K. Termolecular rate coefficients derived from Troe's expression displayed a negative temperature dependence that may be larger than those found for the reactions of OH with isoprene, ethylene, and methyl vinyl ketone under similar conditions although there is considerable uncertainty in these derived low-pressure-limiting rate constants.

Measurements of the rate constant for the OH + MBO reaction in the absence of oxygen at 5 Torr are approximately 10−15% lower than that measured for the OD + MBO reaction, consistent with previous measurements suggesting that elimination of the alcohol OH group occurs from the HO−MBO adduct. Addition of oxygen appears to stabilize the adduct and inhibit alcohol OH elimination, as measurements of the OH + MBO rate constant in the presence of added oxygen are similar to the OD + MBO results.

Theoretical calculations of the energetics of the OH + MBO reaction suggest that the stabilities of the different adducts are similar, with the adduct resulting from OH addition to the internal carbon calculated to be 1−4 kcal mol^{-1} more stable than the adduct formed from OH addition to the terminal carbon. At the B3LYP/6-311+G* + ZPE level of theory, the adducts resulting from addition to the internal and terminal carbons were calculated to be 28.1 and 27.0 kcal mol^{-1} more stable than the reactants, while at the MP2/6-311+G* + ZPE level of theory, addition to the internal and terminal carbons were calculated to be 33.4 and 29.3 kcal mol^{-1} more stable than the reactants, respectively. These stabilization energies result in estimated termolecular rate constants for the OH + MBO reaction using simplified calculations based on RRKM theory that are in reasonable agreement with experimental values between 335 and 415 K. The calculations suggest that the larger negative activation energy for the OH + MBO reaction compared to the OH + isoprene reaction is likely the result of additional low-frequency vibrations in both methylbutenol and the adducts leading to larger temperature dependences of their vibrational partition functions. However, more rigorous calculations are needed to confirm these results.

Although the B3LYP/6-311+G* + ZPE calculated energies predict that OH addition to the internal carbon is slightly more stable than addition to the terminal carbon of methylbutenol, the calculated low-pressure-limiting rate constants using these energies results in a predicted yield of approximately 70% for addition of OH to the terminal carbon, in agreement with previous product studies of this reaction, due to the low-frequency vibrations in this adduct contributing to a larger vibrational partition function that reduces the rate of dissociation. However, the MP2/6-311+G* + ZPE calculated stabilization energies predict that addition to the internal carbon should be preferred due to its greater stability relative to addition to the terminal carbon. Clearly additional theoretical and experimental studies of the OH-initiated oxidation of methylbutenol are needed to resolve these discrepancies.

Acknowledgment. This work is supported by the National Science Foundation and in part by Shared University Research grants from IBM, Inc. to Indiana University.

Supporting Information Available: Geometries, energies, and vibrational frequencies of all structures in this study are available in a separate document. This material is available free of charge via the Internet at http://pubs.acs.org.

References and Notes

(1) Harley, P.; Fridd-Stroud, V.; Greenberg, J.; Guenther, A.; Vasconcellos, P. *J. Geophys. Res.-Atmos.* **1998**, *103*, 25479.

(2) Goldan, P. D.; Kuster, W. C.; Fehsenfeld, F. C.; Montzka, S. A. *Geophys. Res. Lett.* **1993**, *20*, 1039.

(3) Guenther, A.; Geron, C.; Pierce, T.; Lamb, B.; Harley, P.; Fall, R. *Atmos. Environ.* **2000**, *34*, 2205.

(4) Grosjean, E.; Grosjean, D. *Int. J. Chem. Kinet.* **1994**, *26*, 1185.

(5) Hallquist, M.; Langer, S.; Ljungstrom, E.; Wangberg, I. *Int. J. Chem. Kinet.* **1996**, *28*, 467.

(6) Rudich, Y.; Talukdar, R. K.; Fox, R. W.; Ravishankara, A. R. *J. Phys. Chem.* **1996**, *100*, 5374.

(7) Rudich, Y.; Talukdar, R.; Burkholder, J. B.; Ravishankara, A. R. *J. Phys. Chem.* **1995**, *99*, 12188.

(8) Fantechi, G.; Jensen, N. R.; Hjorth, J.; Peeters, J. *Int. J. Chem. Kinet.* **1998**, *30*, 589.

(9) Papagni, C.; Arey, J.; Atkinson, R. *Int. J. Chem. Kinet.* **2001**, *33*, 142.

(10) Imamura, T.; Iida, Y.; Obi, K.; Nagatani, I.; Nakagawa, K.; Patroescu-Klotz, J.; Hatakeyama, S. *Int. J. Chem. Kinet.* **2004**, *36*, 379.

(11) Alvarado, A.; Tuazon, E. C.; Aschmann, S. M.; Arey, J.; Atkinson, R. *Atmos. Environ.* **1999**, *33*, 2893.

(12) Fantechi, G.; Jensen, N. R.; Hjorth, J.; Peeters, J. *Atmos. Environ.* **1998**, *32*, 3547.

(13) Ferronato, C.; Orlando, J. J.; Tyndall, G. S. *J. Geophys. Res.-Atmos.* **1998**, *103*, 25579.

(14) Reisen, F.; Aschmann, S.; Atkinson, R.; Arey, J. *Environ. Sci. Technol.* **2003**, *37*, 4664.

(15) Eisele, F. L.; Tanner, D. J.; Cantrell, C. A.; Calvert, J. G. *J. Geophys. Res.-Atmos.* **1996**, *101*, 14665.

(16) Stevens, P. S.; Mather, J. H.; Brune, W. H.; Eisele, F.; Tanner, D.; Jefferson, A.; Cantrell, C.; Shetter, R.; Sewall, S.; Fried, A.; Henry, B.; Williams, E.; Baumann, K.; Goldan, P.; Kuster, W. *J. Geophys. Res.-Atmos.* **1997**, *102*, 6379.

(17) George, L. A.; Hard, T. M.; O'Brien, R. J. *J. Geophys. Res.-Atmos.* **1999**, *104*, 11643.

(18) Kanaya, Y.; Sadanaga, Y.; Matsumoto, J.; Sharma, U. K.; Hirokawa, J.; Kajii, Y.; Akimoto, H. *J. Geophys. Res.-Atmos.* **2000**, *105*, 24205.

(19) Carslaw, N.; Creasey, D. J.; Harrison, D.; Heard, D. E.; Hunter, M. C.; Jacobs, P. J.; Jenkin, M. E.; Lee, J. D.; Lewis, A. C.; Pilling, M. J.; Saunders, S. M.; Seakins, P. W. *Atmos. Environ.* **2001**, *35*, 4725.

(20) Tan, D.; Faloona, I.; Simpas, J. B.; Brune, W.; Shepson, P. B.; Couch, T. L.; Sumner, A. L.; Carroll, M. A.; Thornberry, T.; Apel, E.; Riemer, D.; Stockwell, W. *J. Geophys. Res.-Atmos.* **2001**, *106*, 24407.

(21) Chuong, B.; Stevens, P. S. *J. Phys. Chem. A* **2000**, *104*, 5230.

(22) Frisch, M. J.; Trucks, G. W.; Schlegel, H. B.; Scuseria, G. E.; Robb, M. A.; Cheeseman, J. R.; Montgomery, J. J. A.; Vreven, T.; Kudin, K. N.; Burant, J. C.; Millam, J. M.; Iyengar, S. S.; Tomasi, J.; Barone, V.; Mennucci, B.; Cossi, M.; Scalmani, G.; Rega, N.; Petersson, G. A.; Nakatsuji, H.; Hada, M.; Ehara, M.; Toyota, K.; Fukuda, R.; Hasegawa, J.; Ishida, M.; Nakajima, T.; Honda, Y.; Kitao, O.; Nakai, H.; Klene, M.; Li, X.; Knox, J. E.; Hratchian, H. P.; Cross, J. B.; Bakken, V.; Adamo, C.; Jaramillo, J.; Gomperts, R.; Stratmann, R. E.; Yazyev, O.; Austin, A. J.; Cammi, R.; Pomelli, C.; Ochterski, J. W.; Ayala, P. Y.; Morokuma, K.; Voth, G. A.; Salvador, P.; Dannenberg, J. J.; Zakrzewski, V. G.; Dapprich, S.; Daniels, A. D.; Strain, M. C.; Farkas, O.; Malick, D. K.; Rabuck, A. D.; Raghavachari, K.; Foresman, J. B.; Ortiz, J. V.; Cui, Q.; Baboul, A. G.; Clifford, S.; Cioslowski, J.; Stefanov, B. B.; Liu, G.; Liashenko, A.; Piskorz, P.; Komaromi, I.; Martin, R. L.; Fox, D. J.; Keith, T.; Al-Laham, M. A.; Peng, C. Y.; Nanayakkara, A.; Challacombe, M.; Gill, P. M. W.; Johnson, B.; Chen, W.; Wong, M. W.; Gonzalez, C.; Pople, J. A. *Gaussian 03*, revision B.05; Gaussian, Inc.: Wallingford, CT, 2004.

(23) Howard, C. J. *J. Phys. Chem.* **1979**, *83* (1), 3.

(24) Chuong, B.; Stevens, P. S. *J. Phys. Chem. A* **2003**, *107*, 2185.

(25) Chuong, B.; Davis, M.; Edwards, M.; Stevens, P. S. *Int. J. Chem. Kinet.* **2002**, *34*, 300.

(26) Troe, J. *J. Chem. Phys.* **1977**, *66*, 4758.

(27) Troe, J. *J. Phys. Chem.* **1979**, *83*, 114.

(28) Donahue, N. M.; Dubey, M. K.; Mohrschladt, R.; Demerjian, K. L.; Anderson, J. G. *J. Geophys. Res.-Atmos.* **1997**, *102*, 6159.

(29) Troe, J. *J. Chem. Phys.* **1977**, *66*, 4745.

(30) Patrick, R.; Golden, D. M. *Int. J. Chem. Kinet.* **1983**, *15*, 1189.

(31) Stevens, P. S.; Seymour, E.; Li, Z. *J. Phys. Chem. A* **2000**, *104*, 5989.

(32) Whitten, G. Z.; Rabinovitch, B. S. *J. Chem. Phys.* **1963**, *38*, 2466.

(33) Singleton, D. L.; Cvetanovic, R. J. *J. Am. Chem. Soc.* **1976**, *98*, 6812.

(34) Alvarez-Idaboy, J. R.; Mora-Diez, N.; Vivier-Bunge, A. *J. Am. Chem. Soc.* **2000**, *122*, 3715.

(35) Greenwald, E. E.; North, S. W.; Georgievskii, Y.; Klippenstein, S. J. *J. Phys. Chem. A* **2005**, *109*, 6031.